Makara Journal of Science

Volume 27
Issue 2 *June*

Article 2

6-25-2023

Application of Photoacoustic Imaging for Pneumonia Detection

Caesarany Maqfiroh
Department of Physics, Faculty of Mathematics and Natural Sciences, Universitas Gadjah Mada, Yogyakarta 55281, Indonesia

Rini Widyaningrum
Department of Dentomaxillofacial Radiology, Faculty of Dentistry, Universitas Gadjah Mada, Yogyakarta 55281, Indonesia

Ahmad Mujtahid Anas
Department of Physics, Faculty of Mathematics and Natural Sciences, Universitas Gadjah Mada, Yogyakarta 55281, Indonesia

Mitrayana Mitrayana
Department of Physics, Faculty of Mathematics and Natural Sciences, Universitas Gadjah Mada, Yogyakarta 55281, Indonesia, mitrayana@ugm.ac.id

Recommended Citation

Maqfiroh, Caesarany; Widyaningrum, Rini; Anas, Ahmad Mujtahid; and Mitrayana, Mitrayana (2023) "Application of Photoacoustic Imaging for Pneumonia Detection," *Makara Journal of Science*: Vol. 27: Iss. 2, Article 2.
DOI: 10.7454/mss.v27i2.1423
Available at: https://scholarhub.ui.ac.id/science/vol27/iss2/2

Makara Journal of Science, 27/2 (2023), 89–96
doi: 10.7454/mss.v27i2.1423

Application of Photoacoustic Imaging for Pneumonia Detection

Caesarany Maqfiroh[1], Rini Widyaningrum[2], Ahmad Mujtahid Anas[1], and Mitrayana[1*]

1. Department of Physics, Faculty of Mathematics and Natural Sciences, Universitas Gadjah Mada, Yogyakarta 55281, Indonesia
2. Department of Dentomaxillofacial Radiology, Faculty of Dentistry, Universitas Gadjah Mada, Yogyakarta 55281, Indonesia

[*]*E-mail: mitrayana@ugm.ac.id*

Received September 14, 2022 | Accepted March 26, 2023

Abstract

We used photoacoustic imaging (PAI) to visualize and compare acoustic intensity levels in pneumonia-affected and healthy chicken lungs. After histological confirmation of pneumonia, the samples were scanned and subjected to a 532-nm diode laser in a photoacoustic imaging system. The acoustic intensity level of pneumonia-affected tissue was examined and compared with that of healthy lung samples. The optimum laser frequency and duty cycle for imaging the samples were 17 kHz and 30%, respectively. The acoustic intensity levels of pneumonia-affected tissue and healthy lungs were −82.5 ± 1.8 dB and −79.9 ± 1.3 dB, respectively. We found that a simple PAI device consisting of a diode laser and condenser microphone could distinguish between pneumonia-affected and healthy lungs. Pneumonia-affected lungs produced less acoustic intensity than that healthy lungs, as supported by histological studies.

Keywords: acoustic, imaging, intensity, photoacoustic, pneumonia

Introduction

Pneumonia is a lung infection that inflames the alveoli in one or both lungs. The disease is manifested by mucus build-up in the lungs, which prevents the exchange of oxygen and carbon dioxide. Consolidation or the filling of alveoli with inflammatory fluids—such as inflammatory exudates, bacteria, and white blood cells—precedes the disease infectious phase and is followed by red hepatization within a few days. Consequently, the lungs become hyperemic and alveolar capillaries engorge with blood. Subsequently, gray hepatization occurs and is followed by resolution. Although pneumonia can be diagnosed early during consolidation or red hepatization stages, the diagnosis is commonly performed using histopathology, which is invasive [1, 2].

Photoacoustic imaging is a non-invasive multimodal technique that uses a pulse laser as its excitation source. The technique combines optical and ultrasonic approaches to overcome the limitations of pure optical imaging and pure ultrasonic imaging posed by significant light scattering in tissues and low contrast and speckles (image artifacts), respectively [3]. PAI is used to assess specific tissue components (chromophores), such as hemoglobin, oxy-hemoglobin, melanin, bilirubin, lipids, and water [4]. Because photoacoustic imaging does not generate ionizing radiation, it has enormous potential in biomedical applications [3].

Photoacoustic effect occurs when light interacts with materials or tissues, which generate photoacoustic signals. When a laser pulse contacts a material or tissue, a small amount of energy is absorbed and transformed to heat [5]. The increase in tissue temperature causes thermoelastic expansion. Furthermore, pressure changes propagate as acoustic waves, which can be monitored on tissue surface, allowing the position of light absorption to be determined and information of the underlying tissue to be obtained [6].

Several *in vitro*, *in vivo*, and *ex vivo* studies have demonstrated the potential of PAI for biomedical applications. Pre-clinical investigations and clinical trials involving photoacoustic techniques have provided several new opportunities for high-resolution visualization of blood vessels in dermatology [7], oncology [8], ophthalmology [9], and neurology [10].

Previous studies have shown that a basic photoacoustic imaging system could be constructed using a modulated diode laser and condenser microphone [11, 12]. We aimed to determine whether a simple PAI system, consisting of a diode laser and a condenser microphone,

could be used to visualize and compare acoustic intensity levels between pneumonia-affected and healthy lungs.

Methods

Materials. This work was approved by the Committee of Health Research, Faculty of Dentistry-Dental Hospital of Universitas Gadjah Mada, Indonesia (Ref:203/KE/FKG-UGM/EC/2022). Pneumonia-affected and healthy lungs were acquired from a chicken abattoir. Samples were fixed in 10% buffered formalin for 24 h. The samples were dissected in half along the median line and embedded in paraffin. Histological examinations were performed on 50% of samples, while the rest were flattened using a microtome and scanned using a PAI system. Figure 1 shows the flow chart of the study.

The PAI system was tested to ensure all components worked properly, including characterizing the Behringer Omni-series condenser microphone ECM8000, stepper motor, and diode laser power (wavelength = 532 nm). Figure 2 illustrates the PAI system [13] that was adapted from our previous study [11].

In a PAI system, condenser microphones function as detectors. Condenser microphones were characterized using the LabView Version 16.0 application (Labview full development system, Ireland) on a computer. The Audio Function Generator GW Instek GFG-8250A series was configured over a 1 kHz–20 kHz frequency range, and acoustic data from the microphone were analyzed using LabView.

In this study, the stepper motor was a vital component of the custom-built X–Y stage. Stepper motor characterization, performed using scan shift commands in LabView, ensured that sample movements in X- and Y-stages were accurate. Finally, diode laser power characterization was performed using a power meter detector and LabView to ensure laser power stability during sample scanning procedures.

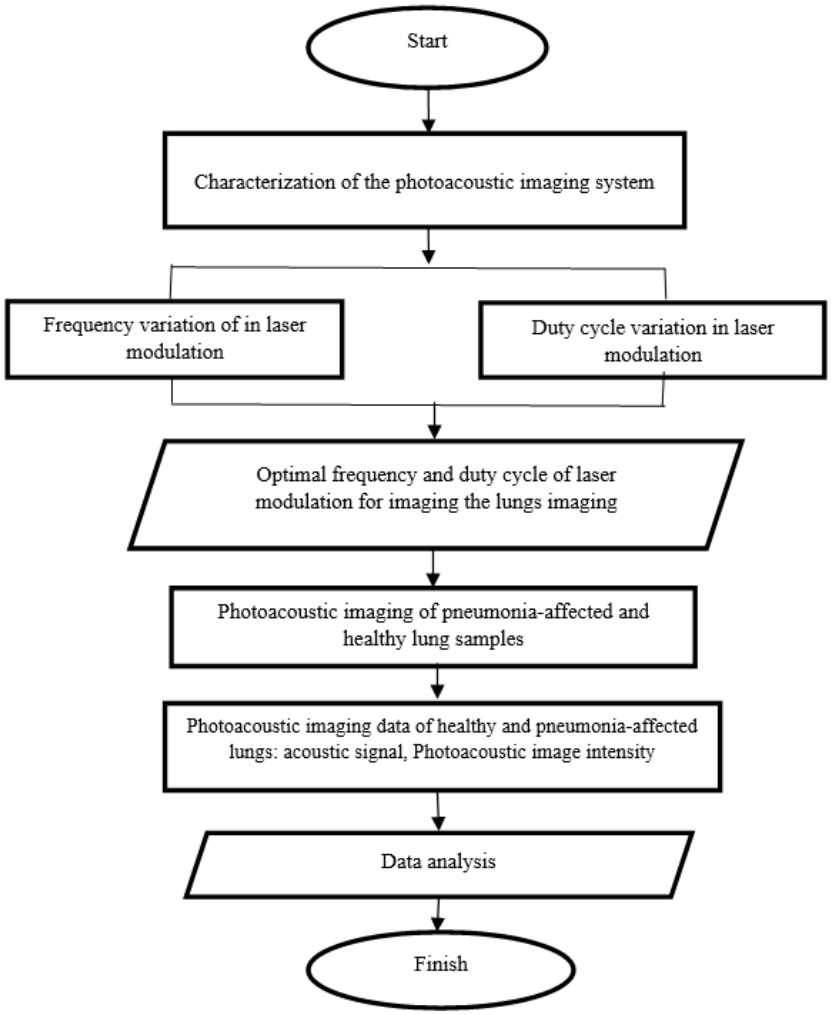

Figure 1. Flowchart of the Study

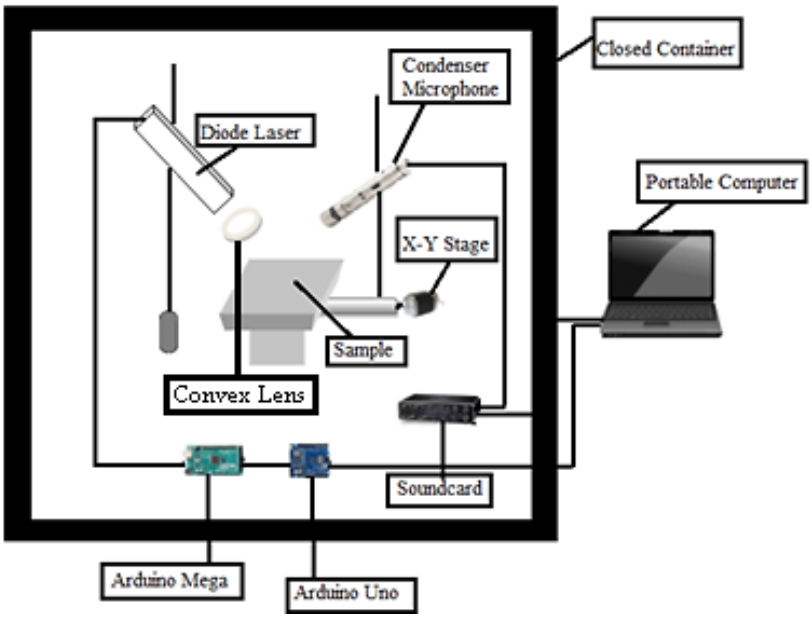

Figure 2. Photoacoustic Imaging System Utilized in the Study [13]

Variations in frequency and duty cycle for optimal laser modulation. We aimed to assess the optimal laser modulation frequency and duty cycle for imaging lung tissue to distinguish between samples and media and acquire information on healthy and pneumonia-infected tissue. The laser frequency was modulated at 16 kHz–20 kHz, with duty cycles of 10%, 20%, 30%, 40%, and 50%.

Photoacoustic imaging of healthy and pneumonia-affected lungs. Samples were scanned to generate photoacoustic images. A sample was placed on a scanning table and exposed to diode laser light, with the condenser microphone placed close to the sample. Scanning was completed using LabView. Acoustic signals from samples were recorded by the microphone, and the signals were converted into photoacoustic images using LabView.

Data normality and statistical test. The data normality test aims to analyze the data distribution in a study. In this study, the normality test for data on the acoustic intensity level of pneumonia and healthy lungs was carried out using the Shapiro Wilk test because the number of samples used was small (less than 50 data). This study tested the research hypothesis using the Mann Whitney nonparametric statistical analysis approach because the data were not normally distributed. The Mann-Whitney statistical test was carried out to test the differences in the samples used in the study.

Results and Discussion

Characterizing the PAI system. Figure 3 shows a linear relationship between the generator's frequency and the condenser microphone frequency (R^2 = 1.00). Thus, the condenser microphone displayed high precision and was an appropriate acoustic signal detector.

To generate photoacoustic images, the sample was positioned using an X–Y stage. A stepper motor drove the stage, moving it in two directions: X (X-stage) and Y (Y-stage). The stepper motor movement was characterized to ensure that X–Y stage shifts were accurate and that photoacoustic images accurately represented target objects. The stepper motor characterization results are shown in Figure 4. The X-stage equation was y = 0.17 + 0.2x, while the Y-stage equation was y = 0.48 + 0.2x. Each 0.2 mm step, as instructed by LabView, resulted in a 0.2 mm shift of X- and Y-stages, with 0.1 mm uncertainty (R^2 = 0.99). These results indicated that the stepper motor shifted accurately.

As shown in Figure 5, the laser power stabilized at 32 mW after 24 min. Thus, photoacoustic imaging and data collection were conducted at 24 min after the laser was switched on to ensure consistency.

Frequency and duty cycle variations for optimal laser modulation. The experimental data of the study are shown in Figure 6. Accordingly, the best PAI frequency for lung tissue was 17 kHz, with an intensity level of −77.11 dB for pneumonia-affected and −76.34 dB for healthy samples.

As shown in Figure 7, our photoacoustic system can identify optimum sound intensity levels of the sample at a duty cycle of 30%, with intensity levels of −80.75 dB for pneumonia-affected and −79.69 dB for healthy samples.

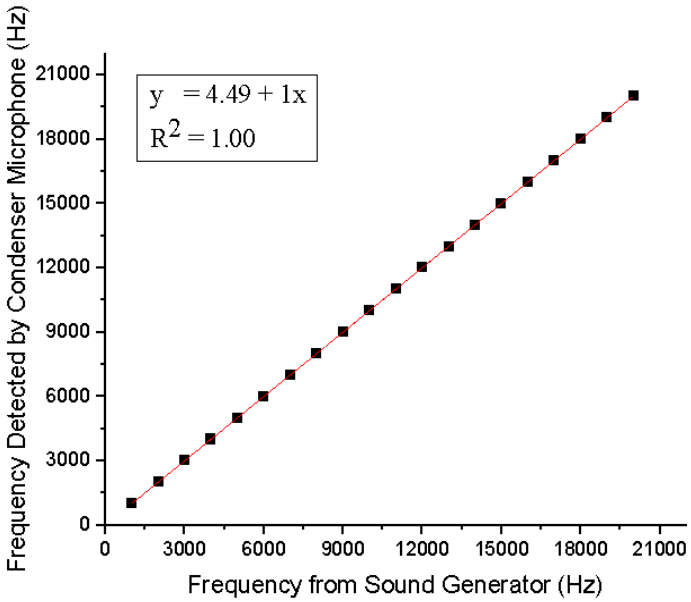

Figure 3. Relationship between the Generator's Frequency and the Condenser Microphone Frequency

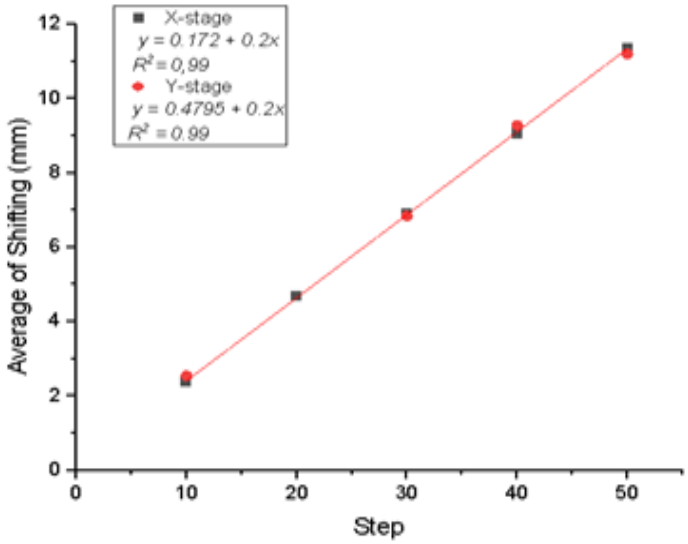

Figure 4. Result of X–Y Stage Characterization

Modulation frequency settings and appropriate duty cycles in pneumonia-affected and healthy lung samples are shown in Figures 6 and 7, respectively. Figure 6, the acoustic intensity was proportional to the laser modulation frequency and directly proportional to absorbed sample energy. Also, the laser modulation duty cycle was related to laser intensity which generated thermal expansion in the sample. The intensity levels peaked at 17 kHz when compared with those at other frequencies. Thus, at this frequency, we could successfully distinguish between pneumonia-affected and healthy lung samples.

Figure 7 shows that the duty cycle influenced acoustic signal generation. Photoacoustic image results were unsatisfactory at 10% and 20% duty cycles due to low acoustic intensity in samples, while at cycles ranging from 40%–50%, samples were at the risk of burning. Furthermore, samples had degraded. Our photoacoustic imaging system imaged pneumonia-affected and healthy lungs at 17 kHz with a 30% duty cycle (Figure 8). The system generated a maximum sound intensity level and represented lung samples at specified frequencies and duty cycles. The frequency and duty cycle of laser irradiation are known to influence acoustic signal generation from samples (Figures 6 and 7) [14].

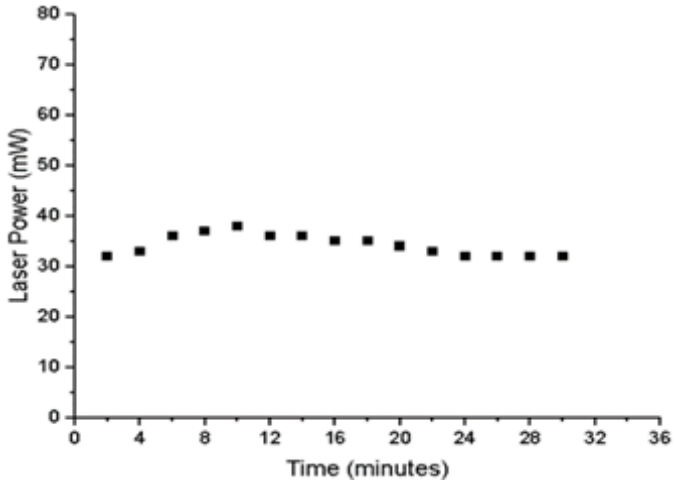

Figure 5. Relationship between Time and Laser Power in the Study. The Wavelength and Duty Cycle of Diode Laser was 532 nm and 30%

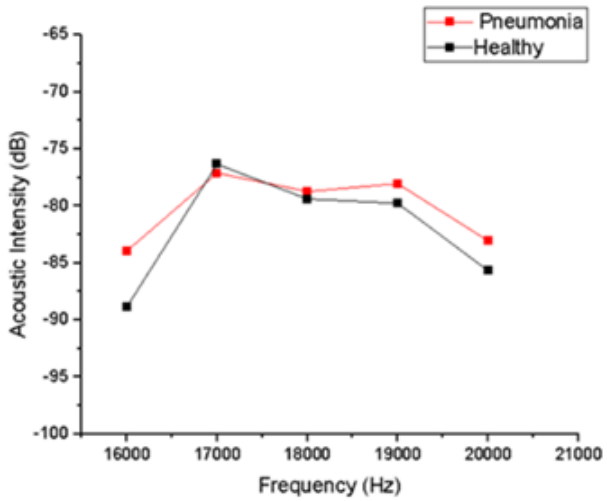

Figure 6. Optimal Frequency for Imaging Lung Tissue

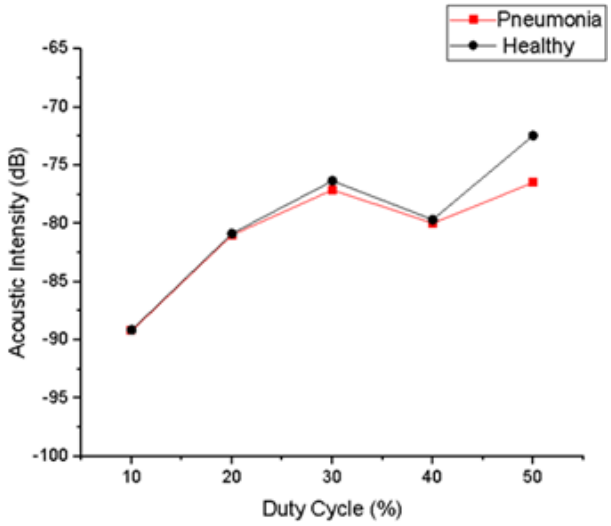

Figure 7. Optimal Duty Cycle for Imaging Lung Tissue

Photoacoustic imaging of pneumonia-affected and healthy lungs. In Figure 8, panels a-1 and a-2 show tissue sample images of pneumonia-affected and healthy lungs. Panels b-1 and b-2 show photoacoustic images in three distinct colors: red, yellow, and blue. Blue indicates the paraffin medium used in samples, while yellow and red indicate the lung tissues. Acoustic signals in pneumonia-affected lung tissue were lower compared with those in healthy lung tissues.

Table 1. Acoustic Intensity Level of Lung Samples

Sample	Acoustic intensity level (dB)
Pneumonia	−82.54
Healthy	−79.92

Acoustic data from six pneumonia-affected and healthy lung samples are shown in Table 1. Substantial variations in acoustic intensity levels were observed between pneumonia-affected and healthy lung samples. The typical lung contains considerable quantity of air, with alveoli possessing small blood veins for gas exchange. However, during pneumonia, the lungs are filled with blood and edematous fluid. Thus, the density of the affected tissues increase because of the increased blood cells in the alveoli during red hepatization [1]. As a result, acoustic intensity levels dropped from −79.9 ± 1.3 dB to −82.5 ± 1.8 dB. We hypothesized that pneumonia-affected lung tissue thickening altered chromophore composition, thereby showing reduced sound intensity levels detected by the microphone. Histopathological examination revealed a thickening of the parabronchial region with substantial infiltration of lymphocytic inflammatory cells (Figure 9).

Radiant light absorption by chromophores forms the basis for PAI in biological tissues. Through photoacoustic effects, chromophores trigger acoustic waves in the tissue via contraction and thermal expansion events [15], [16]. Chromophore concentration in the tissue determines the strength of the photoacoustic output signal, which is subsequently used to reconstruct photoacoustic images [17–19].

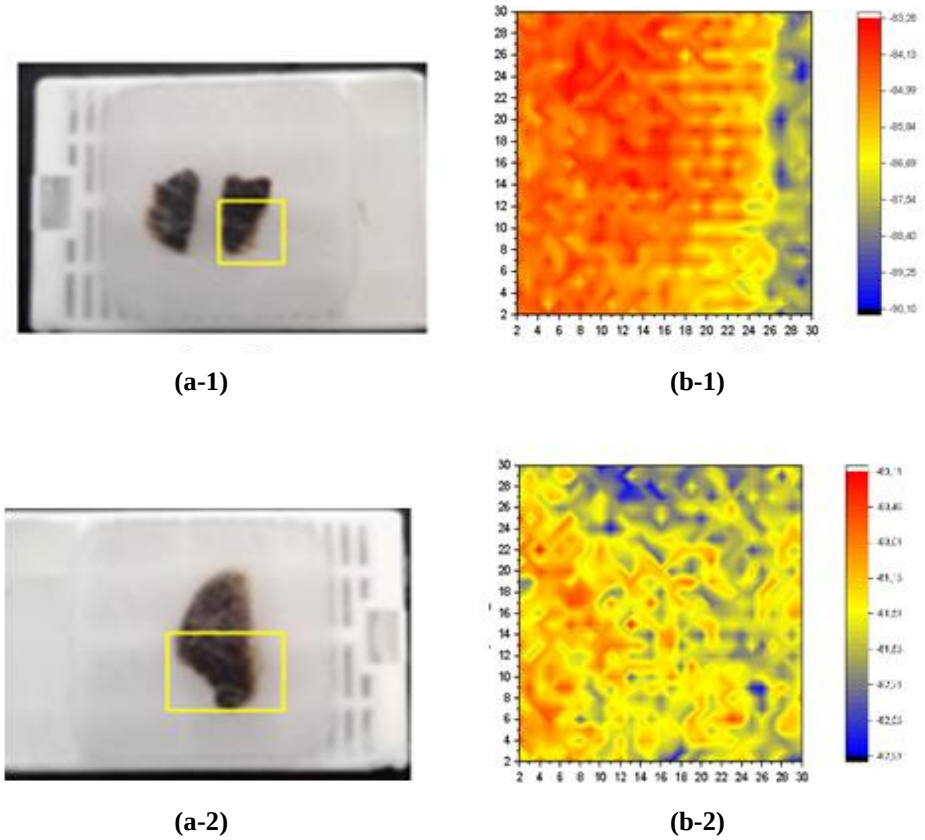

(a-1) **(b-1)**

(a-2) **(b-2)**

Figure 8. Pictures of (a-1) Pneumonia-affected and (a-2) Healthy Lung Samples, and Photoacoustic Image and Acoustic Intensity Levels of (b-1) Pneumonia-affected and (b-2) Healthy Lung Samples. The Yellow Box Shows a Section of a Chicken Lung Scanned Using the PAI System

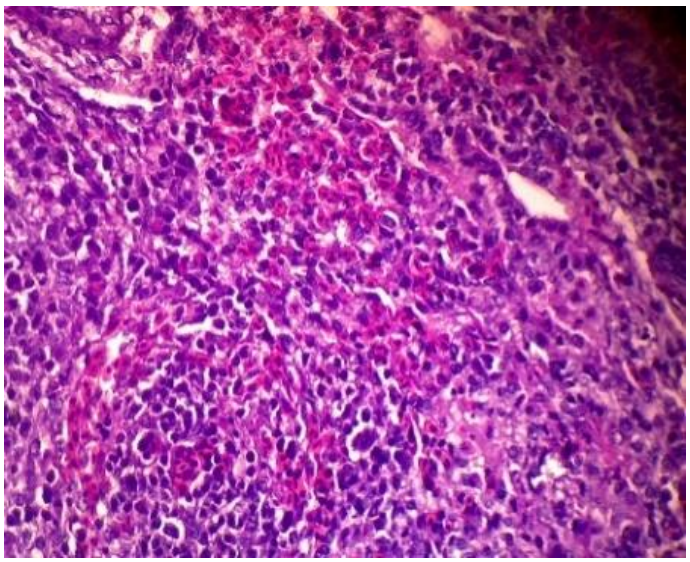

Figure 9. Pneumonia-infected Lungs Showing Lobe-thickening at the Periphery and Lymphocyte Infiltration in the Parabronchus

Tissue density influences photoacoustic absorption and generates different absorption coefficients in different tissues. Endogenous chromophores, such as hemoglobin, melanin, water, and lipids, may absorb laser light and generate acoustic waves in biological tissues [20]. Acoustic intensity levels are affected by tissue density and absorption coefficients. Lower absorption results in a lower acoustic intensity level, indicating a denser tissue [21]. The amplitude of the photoacoustic signals is affected by optical, mechanical, and thermal properties of the object as well as the electromagnetic source radiation [22–24].

Figure 8 depicts the photoacoustic images obtained from the PAI system. The PAI system could distinguish between biological tissue and non-biological materials. In our previous study, we had reported that blue in photoacoustic images represented non-biological materials because of low acoustic signals, whereas yellow and red represented biological tissue because of higher acoustic signals. In the present study, yellow and red represented lung tissue, while blue represented paraffin. This color contrast between different materials suggested that biological tissue had different mechanical, optical, and thermal qualities when compared with those of non-biological materials [22].

Acoustic intensity levels between pneumonia-affected and healthy lung samples were compared using Shapiro Wilk test followed by Mann Whitney *U* test. The former test indicated that acoustic intensity levels were not normally distributed, and therefore Mann–Whitney test was used. The *p*-value (asymp. sig.) was 0.037 ($p < 0.05$); thus, we identified statistically significant differences between pneumonia-affected and healthy lung samples.
We demonstrated that photoacoustic imaging systems based on diode lasers and condenser microphones are highly sensitive to tissue characteristics. Thus, our approach can be used to diagnose numerous diseases and pathological conditions.

Conclusions

We showed that a simple PAI device could be used to distinguish between pneumonia-affected and healthy lung tissues. Pneumonia-affected lungs produced less acoustic intensity levels than those of healthy lungs. A diode laser and condenser microphone can be used to construct and control a photoacoustic system using Lab-View and Arduino Integrated Development Environment on a computer. However, further research is required to develop feasible PAI systems to characterize pneumonia and other diseases.

Acknowledgments

Under the supervision of the co-authors, this work is part of the thesis for the first author's final project. We would like to thank Universitas Gadjah Mada for supporting this research under the grant of Final Project Recognition Program 2022 (No: 3550/UN1.P.III/Dit-Lit/PT.01.05/2022).

References

[1] Biswas, D., Kumari, A., Chen, G.C.K., Vasudevan, S., Gupta, S., Shukla, S., *et al*. 2017. Quantitative Differentiation of Pneumonia from Normal Lungs: Diagnostic Assessment Using Photoacoustic Spectral Response. Appl. Spectro. 71(11): 2532–2537, https://doi.org/10.1177/0003702817708320.

[2] Warganegara, E. 2017. Pneumonia Nosokomial (Hospital-Acquired, Ventilator-Associated, dan Health Care-Associated). Jurnal Kedokteran Universitas Lampung. 1(3): 612–618, https://doi.org/10.23960/jkunila13612-618.

[3] Su, Y., Zhang, F., Xu, K., Yao, J., Wang, R.K. 2005. A photoacoustic tomography system for imaging of biological tissues. J. Phys. D. Appl. Phys. 38(15): 2640–2644, https://doi.org/10.1088/0022-3727/38/15/016.

[4] Sandström, A. 2010. A Historical Review. In Sandström, A. (eds.), Handbook of Solvency for Actuaries and Risk Managers, 1st ed. Chapman and Hall/CRC. London. pp. 67–82.

[5] El-Sharkawy, Y.H., El Sherif, A.F. 2012. Photoacoustic diagnosis of human teeth using interferometric detection scheme. Opt. Laser Technol. 44(5): 1501–1506, https://doi.org/10.1016/j.optlastec.2011.12.009.

[6] Yin, B., Xing, D., Wang, Y., Zeng, Y., Tan, Y., Chen, Q. 2004. Fast photoacoustic imaging system based on 320-element linear transducer array. 49(7): 1339–1346, https://doi.org/10.1088/0031-9155/49/7/019.

[7] Kratkiewicz, K., Manwar, R., Rajabi-Estarabadi, A., Fakhoury, J., Meiliute, J., Daveluy, S., *et al*. 2019. Photoacoustic/Ultrasound/Optical Coherence Tomography Evaluation of Melanoma Lesion and Healthy Skin in a Swine Model. Sensors. 19(12): 2815, https://doi.org/10.3390/s19122815.

[8] Valluru, K.S., Wilson, K.E., Willmann, J.K. 2016. Photoacoustic Imaging in Oncology: Translational Preclinical and Early Clinical Experience. Radiology. 280(2): 332–349, https://doi.org/10.1148/radiol.16151414.

[9] Wang, L.V., Yao, J. 2016. A practical guide to photoacoustic tomography in the life sciences. Nat. Method. 13: 627–638, https://doi.org/10.1038/nmeth.3925.

[10] Liu, Y.H., Xu, Y., Liao, L.-D., Chan, K.C., Thakor, N.V. 2018. A handheld real-time photoacoustic imaging system for animal neurological disease models: From simulation to realization. Sensors. 18(11): 4081, https://doi.org/10.3390/s18114081.

[11] Widyaningrum, R., Agustina, D., Mudjosemedi, M., Mitrayana. 2018. Photoacoustic for oral soft tissue

imaging based on intensity modulated continuous-wave diode laser. Int. J. Adv. Sci. Eng. Inf. Technol. 8(2): 622–627, https://doi.org/10.18517/ijaseit.8.2.2383.

[12] Alifkalaila, A., Mitrayana, Widyaningrum, R. 2021. Photoacoustic Imaging System based on Diode Laser and Condenser Microphone for Characterization of Dental Anatomy. Int. J. Adv. Sci. Eng. Inf. Technol. 11(6): 2363–2368, https://doi.org/10.18517/ijaseit.11.6.12902.

[13] Maqfiroh, C. 2022. Application of Photoacoustic Imaging Based on Diode Laser and Condenser Microphone for Simulation of Pneumonia Detection [Thesis]. Yogyakarta: Universitas Gadjah Mada.

[14] Bageshwar, D., Pawar, A.S., Khanvilkar, V., Kadam, V. 2010. Photoacoustic Spectroscopy and Its Applications-A Tutorial Review. Eurasian J. Anal. Chem. 5: 187–203.

[15] Erfanzadeh, M., Kumavor, P.D., Zhu, Q. 2018. Laser scanning laser diode photoacoustic microscopy system. Photoacoustics. 9: 1–9, https://doi.org/10.1016/j.pacs.2017.10.001.

[16] Zhong, H., Duan, T., Lan, H., Zhou, M., Gao, F. 2018. Review of low-cost photoacoustic sensing and imaging based on laser diode and light-emitting diode. Sensors. 18(7): 2264, https://doi.org/10.3390/s18072264.

[17] Valluru, K.S., Chinni, B.K., Rao, N.A., Bhatt, S., Dogra, V.S. 2009. Basics and Clinical Applications of Photoacoustic Imaging. Ultrasound Clin. 4(3): 403–429, https://doi.org/10.1016/j.cult.2009.11.007.

[18] Laufer, J. 2018. Photoacoustic imaging: Principles and applications. In Sack, I., Schaeffter, T. (eds.), Quantification of Biophysical Parameters in Medical Imaging. Springer, Cham. US. pp. 303–324.

[19] Kalva, S.K., Upputuri, P.K., Rajendran, P., Dienzo, R.A., Pramanik, M. 2019. Pulsed Laser Diode-Based Desktop Photoacoustic Tomography for Monitoring Wash-In and Wash-Out of Dye in Rat Cortical Vasculature. J. Vis. Exp. 147: e59764, https://doi.org/10.3791/59764.

[20] Yao, J., Wang, L., Yang, J.-M., Maslov, K.I., Wong, T.T.W., Li, L., Chih-Hsien, *et al*. 2015. High-speed label-free functional photoacoustic microscopy of mouse brain in action. Nat. Method. 12(5): 407–410, https://doi.org/10.1038/nmeth.3336.

[21] Maslov, K.I., Wang, L.V. 2008. Photoacoustic imaging of biological tissue with intensity-modulated continuous-wave laser. J. Biomed. Opt. 13(2): 024006, https://doi.org/10.1117/1.2904965.

[22] Widyaningrum, R., Gracea, R.S., Agustina, D., Mudjosemedr, M., Mitrayana, M., Silalahi, H.M. 2020. The Influence of Diode Laser Intensity Modulation on Photoacoustic Image Quality for Oral Soft Tissue Imaging. J. Lasers Med. Sci. 11: S92–S100, https://doi.org/10.34172/JLMS.2020.S15.

[23] Beard, P. 2011. Biomedical photoacoustic imaging. Interface Focus. 1(4): 602–631, https://doi.org/10.1098/rsfs.2011.0028.

[24] Zhou, Y., Yao, J., Wang, L.V. 2016. Tutorial on photoacoustic tomography. J. Biomed. Opt. 21(6): 061007, https://doi.org/10.1117/1.jbo.21.6.061007.